Title

Temperature-adaptive radiative coating for all-season household thermal regulation

Journal

Science, 374(6574)

ISSN

0036-8075

Authors

Tang, Kechao
Dong, Kaichen
Li, Jiachen
et al.

Publication Date

2021-12-17

DOI

10.1126/science.abf7136

Peer reviewed

Temperature-adaptive radiative coating for all-season household thermal regulation

Kechao Tang[1,2,3 †], Kaichen Dong[1,2 †], Jiachen Li[1†], Madeleine Gordon[4,5], Finnegan G. Reichertz[6], Hyungjin Kim[2,7], Yoonsoo Rho[8], Qingjun Wang[1,2], Chang-Yu Lin[1], Costas P. Grigoropoulos[8], Ali Javey[2,7], Jeffrey J. Urban[5], Jie Yao[1,2], Ronnen Levinson[9], and Junqiao Wu[1,2,4 *]

Affiliations:

[1]Department of Materials Science and Engineering, University of California, Berkeley, CA, 94720, USA.

[2]Division of Materials Sciences, Lawrence Berkeley National Laboratory, Berkeley, CA, 94720, USA.

[3]Key Laboratory of Microelectronic Devices and Circuits (MOE), Institute of Microelectronics, Peking University, Beijing 100871, P. R. China

[4]Applied Science and Technology Graduate Group, University of California, Berkeley, CA, 94720, USA

[5]The Molecular Foundry, Lawrence Berkeley National Laboratory, Berkeley, CA, 94720, USA

[6]East Bay Innovation Academy, 3800 Mountain Blvd., Oakland, CA, 94619, USA

[7]Department of Electrical Engineering and Computer Sciences, University of California, Berkeley, CA, 94720, USA.

[8]Department of Mechanical Engineering, University of California, Berkeley, CA, 94720, USA.

[9]Heat Island Group, Lawrence Berkeley National Laboratory, Berkeley, CA, 94720, USA.

* Correspondence to: wuj@berkeley.edu

† These authors contributed equally to the work

Abstract:

The sky is a natural heat sink that has been extensively used for passive radiative cooling of households. Past experimental works have focused on maximizing radiative cooling power of roof coating in hot daytime using static, cooling-optimized material properties. However, the resultant overcooling in cold night or winter times exacerbates the heating cost, especially in climates where heating dominates energy consumption. In this work, we approach the thermal regulation from an all-season perspective by developing a mechanically flexible coating that adapts its thermal emittance to different ambient

temperatures. The fabricated temperature-adaptive radiative coating (TARC) automatically switches thermal emittance from 0.20 for ambient temperatures lower than 15 °C to 0.90 for temperatures above 30 °C, driven by a photonically amplified metal-insulator transition. The TARC is simulated to outperform all existing roof coatings for energy saving in most climates, especially those with significant seasonal variations, yielding a minimum cut in annual source energy consumption up to 3.65 GJ in the U.S. for a typical single-family home.

Introduction

More than 40% of the total energy consumption in countries such as the United States is in buildings, and within this portion of energy, about 48% is consumed on heating and cooling to maintain a desirable indoor temperature (about 22 °C).[1] In contrast to most temperature regulation systems that require external power input, the mid-infrared atmospheric transparency window allows thermal radiation from the earth towards the 3 K temperature outer space, thus opening a passive avenue for radiative cooling of buildings. This method to cool an outdoor surface, such as a roof, has been extensively studied in the past,[2-4] and is recently advanced by the development of daytime radiative cooling[5-10] using materials with low solar absorptance and high thermal emittance, in the form of thin films,[7] organic paints,[8] or structural materials.[9]

Past research on daytime radiative cooling, despite their success in reducing cooling energy consumption, typically used materials with fixed, cooling-optimized properties, which efficiently emit thermal radiation even when the temperature of the surface is lower than desired, such as during the night or in the winter. This unwanted thermal radiative cooling will increase the energy consumption for heating, and may offset the cooling energy saved in hot hours or seasons. This issue is well-acknowledged by the research community and mitigation of the over-cooling becomes a timely demand.[11] To cut the heating penalty from over-cooling, a few techniques were recently attempted for switching off thermal radiative cooling at low temperatures (below 22 °C). Although effective in switching, these techniques typically require either additional energy input[12,13] or external activation,[14] and in some cases is achieved by mechanically moving parts.[15,16] It is highly desirable to develop dynamic structures that automatically switch off the radiative cooling at low temperatures. Existing efforts in self-switching radiative cooling, however, are either purely theoretical,[17-20] or limited to materials characterization with little relevance to practical household thermal regulation.[21-24]

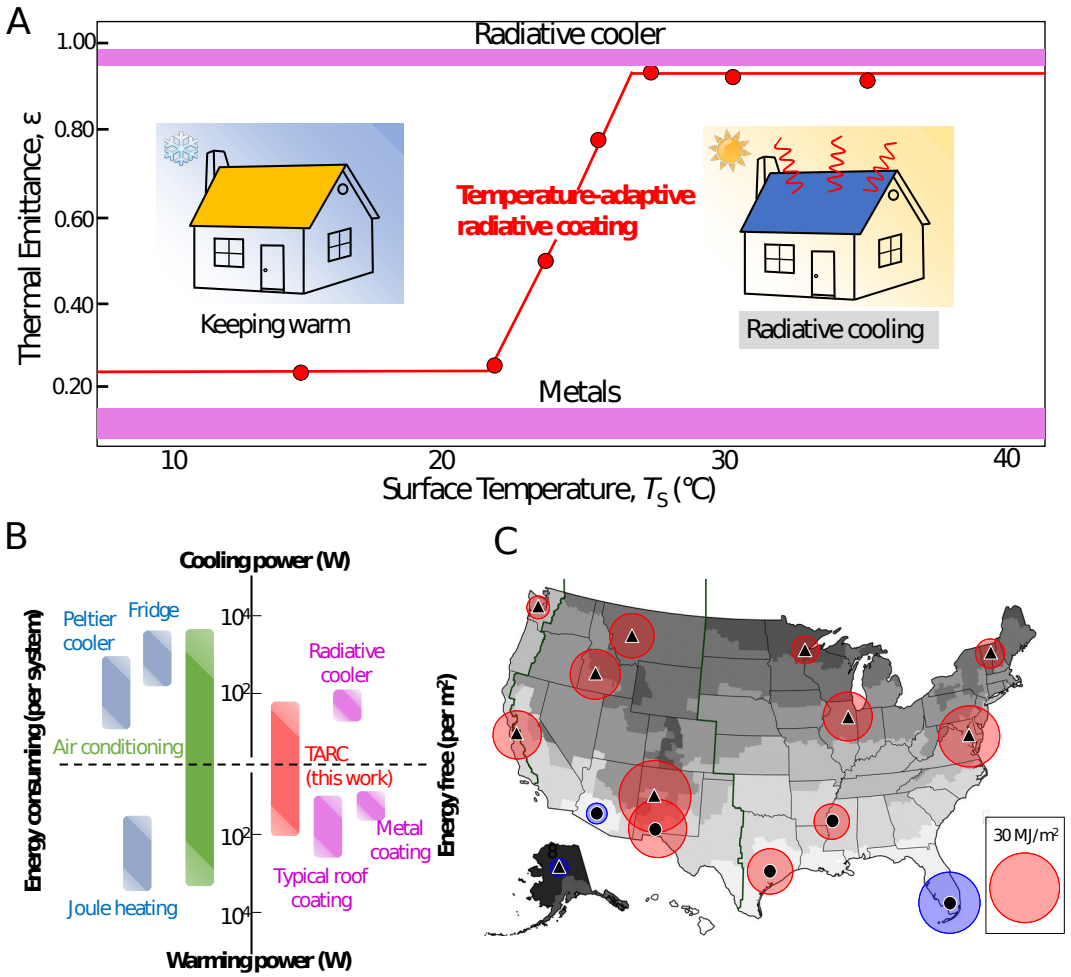

Figure 1. Temperature-adaptive radiative coating (TARC) and its benefits for household thermal regulation. A. Basic property of TARC in thermal emittance modulation and schematics for temperature management when used as a household roof coating. The data points are experimental emittance of a TARC. **B.** TARC in comparison to other thermal regulation systems, highlighting the unique benefit of TARC of being simultaneously energy free and temperature adaptive. **C.** Simulated minimum annual space conditioning source energy saving ($SCSES_{min}$) of TARC compared to other existing roof coating materials for different cities representing the 15 climate zones in the U.S. Red and blue circles indicate positive and negative $SCSES_{min}$ values, respectively. The values are scaled to the area of the circles. Details of the simulation can be found in the Supporting Information.

In this work, we tackle this problem by designing and fabricating a flexible coating structure for all-season household thermal regulation. This temperature-adaptive radiative coating (TARC) automatically switches its thermal emittance to 0.90 from 0.20 when the surface temperature rises above ~22 °C, delivering high radiative cooling power exclusively for the high temperature condition (Fig. 1A). The solar absorptance is also optimized at ~ 0.25 (solar reflectance 0.75) for all-season energy saving in major U.S. cities (Fig. S7), a value comparable to that of a commercial white roof coating. The TARC is the first energy-autonomous and temperature-adaptive thermal regulation system (Fig.1B) to demonstrate effective surface temperature modulation in an outdoor test environment. Extensive simulations were performed based on the device properties and the global climate database, which show advantages of TARC over all existing roof coating materials in energy saving for most U.S. cities in different climate zones and global cities (Fig. 1C and Fig. S8). The energy saving by TARC not only brings economic benefits but also contributes to environmental preservation by cutting off green-house gas emission.

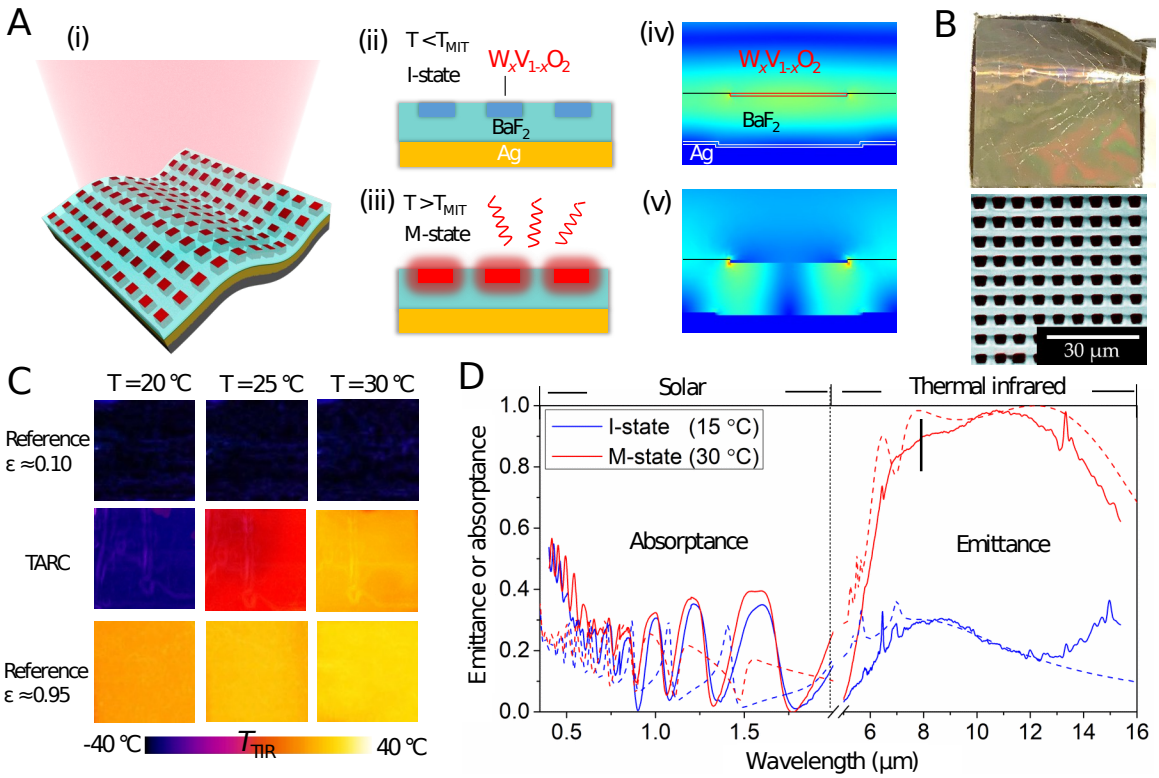

Figure 2. Basic properties of TARC and experimental characterization. A. Schematics of the structure (i), materials composition, and working mechanism (ii - iii) of the TARC. T_{MIT} denotes the metal-insulator transition temperature. Subpanels (iv) and (v) show

the simulated distribution of electric field intensity below and above the transition temperature, respectively, when electromagnetic waves with a wavelength of 7.8 μm were normally incident on the TARC structure. **B.** A photo (2 cm × 2 cm) and an SEM image of a TARC, showing high flexibility and structural consistency with the design. **C.** Thermal infrared (TIR) images of a TARC compared to those of two conventional materials (references) with constantly low or high thermal emittance, showing the temperature-adaptive switching in thermal emittance of TARC. **D.** Solar spectral absorptance and thermal spectral emittance of TARC at a low temperature and a high temperature, measured by a UV-vis-IR spectrometer with integrating sphere and a Fourier transform infrared (FTIR) spectrometer, respectively (solid curves), showing consistency with theoretical predictions (dashed curves). The arrow at 7.8 μm denotes the wavelength where subpanels (iv) and (v) of **A** are simulated.

Basic properties of TARC

The TARC is developed based on the well-known metal-insulator transition (MIT) of the strongly correlated electron materials $W_xV_{1-x}O_2$,[25] and the transition temperature (T_{MIT}) is tailored to about 22 °C by setting the composition x at 1.5%.[26] A lithographically patterned two-dimensional array of thin $W_xV_{1-x}O_2$ blocks are embedded in a BaF_2 dielectric layer which sits on top of an Ag film (Fig. 2A). In the insulating (I) state of $W_xV_{1-x}O_2$ at $T < T_{MIT}$, the material is largely transparent to the IR radiation in the 8-13 μm spectral window, so the incident IR radiation is reflected by the Ag mirror with little absorption.[27] In contrast, the $W_xV_{1-x}O_2$ becomes highly IR absorptive when it switches to the metallic (M) state at $T > T_{MIT}$,[27] and the absorption is further amplified by the designed photonic resonance with adjacent $W_xV_{1-x}O_2$ blocks as well as with the bottom Ag layer via the ¼-wavelength cavity. According to the Kirchhoff's law of radiation,[28] the thermal emittance equals the thermal absorptance and switches from low to high values when the temperature exceeds T_{MIT}. Consequently, strong radiative cooling is turned on in operation exclusively at high temperatures, leaving the system in solar-heating or keep-warm mode at low temperatures. The fabrication process and structural parameters can be found in the Methods section and Fig. S1.

Figure 2B shows optical images of a fabricated TARC with high flexibility for versatile surface adaption, as well as a microscale structure consistent with the design. The global emittance switching was first examined by a thermal infrared camera (Fig. 2C). The TARC surface was imaged together with two reference samples having similar thickness but constantly low thermal emittance (0.10, copper plate) or high thermal emittance (0.95, black carbon-fiber tape), respectively. While the thermal emission of the reference samples appears not strongly temperature sensitive from 20 to 30 °C, the TARC shows a dramatic change, corresponding to the switch in thermal emittance at the MIT around 22 °C.

Spectral properties of the TARC were measured by a UV-vis-IR spectrometer and Fourier-transform infrared spectroscopy (FTIR) for the solar and thermal-IR wavelength regimes, respectively, and are shown in Fig. 2D. The solar absorptance (A, 0.3-2.5 μm) is about 0.25, and the sky-window emittance (ε_s, 8-13 μm) is about 0.20 in the I state and 0.90 in the M state, consistent with theoretical simulations and other characterization results (Fig. S2 and Fig. S3).

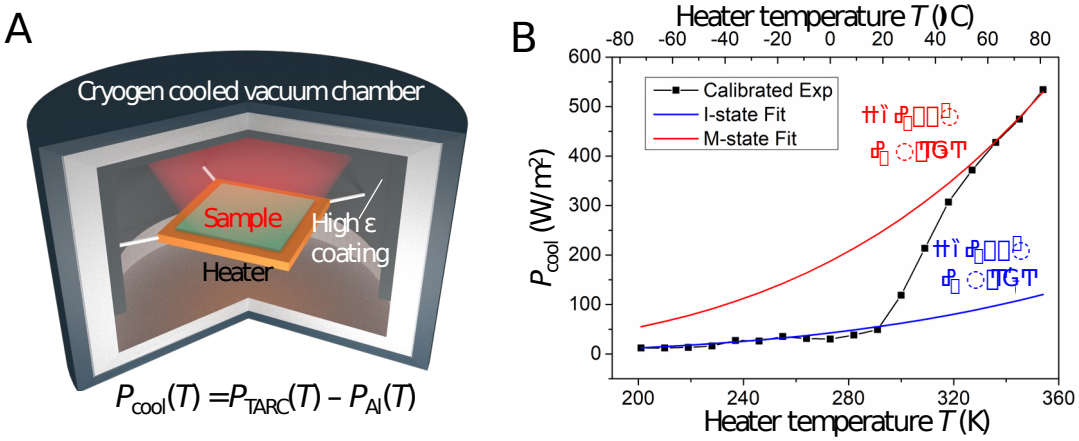

Figure 3. Characterization of intrinsic radiative cooling power of TARC in a cold vacuum chamber. A. Schematics of the experimental setup, showing a thin heater membrane covered by TARC or an Al foil and suspended in a cryogen cooled vacuum chamber. The Al foil reference is used to cancel out the effect of thermal loss via conduction. **B.** Measured areal cooling power of TARC as a function of temperature in vacuum. Fitting of the $P_{cool}(T)$ at I and M states by the Stefan-Boltzmann radiation law gives ε_s equal to 0.20 and 0.90, respectively. -

Characterization of radiative cooling power

The emittance switching of TARC enables modulation of radiative cooling power in response to ambient temperature, which was first measured in vacuum shown in Fig. 3A. A heater membrane was suspended by thin strings in a vacuum chamber, which was cooled with dry ice to -78 °C to minimize radiation from the chamber walls. A piece of Al foil with $\varepsilon_s \approx 0.03$ or an TARC with the same size was attached to the top of the heater in two separate measurements. At each stabilized sample temperature T, the heating powers needed for the two coating scenarios are denoted as $P_{Al}(T)$ and $P_{TARC}(T)$, respectively. The intrinsic cooling power contributed by the TARC was calculated as $P_{cool}(T) = P_{TARC}(T) - P_{Al}(T)$. The Al foil reference was used to calibrate background heat loss from thermal conduction. Figure 3B plots the calibrated cooling power, showing an abrupt increase in $P_{cool}(T)$ when T increases above the MIT temperature. $P_{cool}(T)$ at the I state and M state are well fitted by the Stefan-Boltzmann radiation law, with the thermal emittance extracted to be about 0.20 and 0.90, respectively, consistent with the spectrally characterized results (Fig. 2D). Note that effect of radiation from the chamber wall (about

-78 °C) was accounted for and corrected in the calibration. A constant factor of β ($\approx$ 0.7) is introduced here to account for the difference between the vacuum and ambient measurement conditions (details in Fig. S4).

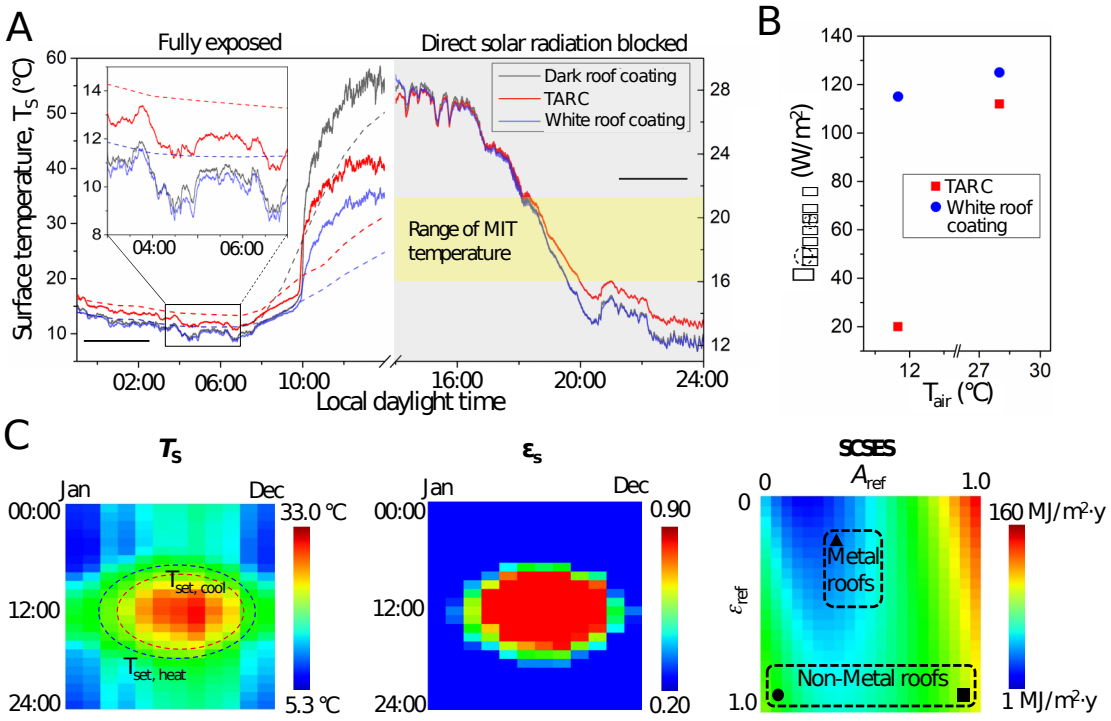

Figure 4. Characterization of TARC in an outdoor environment and calculated thermal load advantage. A. Surface temperature of TARC, a commercial dark roof coating (A = 0.70, ε_s = 0.90), and a commercial white roof coating (A = 0.15, ε_s = 0.90) in an open-space outdoor environment recorded over a day-night cycle. The measurement was taken at 2020-07-05, Berkeley (37.91 °N, 122.28 °W). The solid and dashed curves are experimental data and simulation results based on local weather database, respectively. Measurements starting from 14:00 local daylight time (LDT) were performed with the direct solar radiation blocked. The data after sunset show a clear sign of TARC shutting off radiative cooling as temperature falls below T_{MIT}. **B.** Measured ambient cooling power of TARC and white roof coating with direct solar radiation blocked in the outdoor environment. **C.** Calculated surface temperature (T_s) and the corresponding emittance (ε_s) mapping of TARC over 24 hours and the full year for Berkeley, California, as well as the space conditioning source energy saving (SCSES) of TARC compared to all other materials with fixed solar absorptance (A_{ref}) and thermal emittance (ε_{ref}). The icons in the SCSES map correspond to those used in Fig. 1C, denoting

the optical parameters (A, ε_s) of the strongest rival to TARC in source energy saving for the local climate.

Demonstration of performance in outdoor environment

The actual outdoor performance of the TARC is demonstrated in Fig. 4. The surface temperatures (T_S) of the TARC, together with a dark roof coating product (BEHR #N520 Asphalt Gray) and a cool (white) roof coating product (GAF RoofShield White Acrylic), were recorded over 24 hours on a sunny summer day on a rooftop in Berkeley, California, with a careful design of the measurement system to minimize the effects of artifacts (see Fig. S5).

From 00:00 to 09:00 local daylight time (LDT) when the ambient temperature was below T_{MIT}, the TARC was 2 °C warmer than the two reference roof coatings, arising from the low thermal emittance (ε_s = 0.20) of the TARC in the I-state and thus a lower radiative cooling power than the references (ε_s = 0.90). The 2 °C temperature elevation is consistent with adiabatic simulation results based on these nominal emittance values and the local weather database (see Supporting Information). From 09:00 to 14:00 LDT when the samples were in direct sunlight, T_S was dominated by the solar absorption in balance with radiative cooling and air convection, and the differences between the samples agree with the simulated results assuming the solar absorptance A to be 0.15, 0.25, and 0.70 for the white roof coating, the TARC, and the dark roof coating, respectively. After 14:00 LDT, a shield was erected to intentionally block direct solar radiation to the surface of the samples, which imitates the scenario of a cloud blocking the sun but with the rest of the sky mostly clear. A convergence of the T_s curves was quickly observed for all three samples, an indication that the thermal emittance of the TARC in the M state is close to that of the two references (0.90). This condition persists for a few hours until T_S started to drop below T_{MIT} =¿22 °C. After this point, TARC grew warmer than the two references, with a final temperature difference of about 2 °C similar to the 00:00 to 09:00 LDT period; this indicates that the TARC switched to the low-emittance I state. The 24-hour outdoor experiments demonstrate the emittance switching and resultant temperature regulation by TARC.

To directly compare their ambient condition cooling power ($P_{cool_{amb}}$), the TARC and the white roof coating were heated to the air temperature with the direct solar radiation blocked. $P_{cool_{amb}}$ refers to the power needed to balance the net heat loss from the surface, namely, the thermal radiative heat loss minus the absorbed diffusive solar irradiance power. The obtained $P_{cool_{amb}}$ values at a low and a high air temperature are plotted in Fig. 4B. The TARC exhibits a clear switching of $P_{cool_{amb}}$ by a factor over five across the MIT. This is in stark contrast to the nearly constant $P_{cool_{amb}}$ around 120 W/m^2 for the white roof coating, which is consistent with values (90 - 130 W/m^2) reported in literature for radiative cooling roofs.[4,7,8]

Space-conditioning energy savings potential in U.S. cities

We performed extensive numerical simulations to analyze the performance of TARC in household energy saving for the U.S. and global cities from an all-season perspective.

Details of the simulations are in the Methods section and the Supporting Information. Figure 4C shows the simulated results for Berkeley where the measurements in Fig. 4A & B were carried out. An hour-month map of T_S was calculated using a local weather file, laying the basis for estimation of energy saving. We assume heating and cooling setpoints $T_{set,\,heat}$ = 22 °C and $T_{set,\,cool}$ = 24 °C,[29] and approximate that the building will need heating when $T_s < T_{set,\,heat}$ and require cooling when $T_s > T_{set,\,cool}$. In hour-of-year i, we define heating degrees $D_{h,i} = (T_{set,\,heat} - T_{s,i})_+$ and cooling degrees $D_{c,i} = (T_{s,i} - T_{set,\,cool})_+$, where $x_+ = x$ if $x > 0$ or 0 otherwise. The annual average heating degrees and cooling degrees are denoted by D_h and D_c, respectively.

We used past simulations of cool-roof energy savings to predict potential space-conditioning source energy savings (SCSES) attainable by using TARC in place of roofing materials that have static values of solar absorptance and thermal emittance (Details in the Method section). The figure of merit of TARC is represented by $SCSES_{min}$, the minimum value of SCSES found over existing conventional roofing materials - *i.e.*, roof surfaces with values of A_{ref} and ε_{ref} contained in either of the two boxes shown in Fig. 4C. $SCSES_{min}$ is mapped for cities representing the 15 U.S. climate zones in Fig. 1C, as well as for major global cities in Fig. S8. It can be seen that TARC provides a clear, positive annual space-conditioning source energy savings relative to all existing roof coating materials in most major cities, except for climates that are constantly cold (such as Fairbanks and Reykjavík) or hot (such as Miami and Singapore) all year round. The figure of merit map highlights the advantage of TARC, especially in climate zones with wide temperature variations, day to night or summer to winter. For example, we estimate for a single-family home in Baltimore, MD built before 1980, $SCSES_{min}$ is 22.4 MJ/m^2·y, saving 2.64 GJ/y based on a roof area of 118 m².

The results in both Fig. 1C and Fig. 4C are based on the dominant resident building prototype in the United States,[30] which is a single-family home built prior to 1980. Minimum annual source energy savings per unit roof area for single-family homes and apartment buildings built before 1980, between 1980 and 1999, and recently are presented in Table S4.

Conclusions

A mechanically flexible, energy-autonomous, and temperature-adaptive radiative coating (TARC) is developed for intelligent regulation of household temperature. This system works on the basis of a thermally driven metal insulator transition in cooperation with photonic resonance, and features a self-switching in thermal emittance from 0.20 to 0.90 at a desired temperature of about 22 °C. These unprecedented properties enable switching of the system from radiative cooling mode at high temperatures to solar-heating or keep-warm mode at low temperatures in an outdoor setting. For most cities in the U.S. and around the world, the TARC is predicted to outperform conventional roof materials in cutting energy consumption for households. Combined with the possibility of mass production (Fig. S9), this technology will bring broad benefit of building energy saving and environment preservation.

References

1. Book, B. E. D. Energy efficiency and renewable energy. *US department of energy*, (2011).
2. Gentle, A. R. & Smith, G. B. A subambient open roof surface under the mid-summer sun. *Advanced Science* **2**, 1500119, (2015). <https://doi.org/10.1002/advs.201500119>.
3. Dong, M., Chen, N., Zhao, X., Fan, S. & Chen, Z. Nighttime radiative cooling in hot and humid climates. *Opt. Express* **27**, 31587-31598, (2019). <https://doi.org/10.1364/OE.27.031587>.
4. Orel, B., Gunde, M. K. & Krainer, A. Radiative cooling efficiency of white pigmented paints. *Solar Energy* **50**, 477-482, (1993). <https://doi.org/10.1016/0038-092X(93)90108-Z>.
5. Shi, N. N., Tsai, C.-C., Camino, F., Bernard, G. D., Yu, N. & Wehner, R. Keeping cool: Enhanced optical reflection and radiative heat dissipation in Saharan silver ants. *Science* **349**, 298-301, (2015). <https://doi.org/10.1126/science.aab3564>.
6. Kou, J.-l., Jurado, Z., Chen, Z., Fan, S. & Minnich, A. J. Daytime radiative cooling using near-black infrared emitters. *ACS Photonics* **4**, 626-630, (2017). <https://doi.org/10.1021/acsphotonics.6b00991>.
7. Zhai, Y., Ma, Y., David, S. N., Zhao, D., Lou, R., Tan, G., Yang, R. & Yin, X. Scalable-manufactured randomized glass-polymer hybrid metamaterial for daytime radiative cooling. *Science* **355**, 1062-1066, (2017). <https://doi.org/10.1126/science.aai7899>.
8. Mandal, J., Fu, Y., Overvig, A. C., Jia, M., Sun, K., Shi, N. N., Zhou, H., Xiao, X., Yu, N. & Yang, Y. Hierarchically porous polymer coatings for highly efficient passive daytime radiative cooling. *Science* **362**, 315-319, (2018). <https://doi.org/10.1126/science.aat9513>.
9. Li, T., Zhai, Y., He, S., Gan, W., Wei, Z., Heidarinejad, M., Dalgo, D., Mi, R., Zhao, X., Song, J., Dai, J., Chen, C., Aili, A., Vellore, A., Martini, A., Yang, R., Srebric, J., Yin, X. & Hu, L. A radiative cooling structural material. *Science* **364**, 760-763, (2019). <https://doi.org/10.1126/science.aau9101>.
10. Li, Z., Chen, Q., Song, Y., Zhu, B. & Zhu, J. Fundamentals, materials, and applications for daytime radiative cooling. *Advanced Materials Technologies* **5**, 1901007, (2020). <https://doi.org/10.1002/admt.201901007>.
11. Ulpiani, G., Ranzi, G., Shah, K. W., Feng, J. & Santamouris, M. On the energy modulation of daytime radiative coolers: A review on infrared emissivity dynamic switch against overcooling. *Solar Energy* **209**, 278-301, (2020). <https://doi.org/10.1016/j.solener.2020.08.077>.
12. Goncharov, K., Orlov, A., Tarabrin, A., Gottero, M., Perotto, V., Tavera, S. & Zoppo, G. P. 1500 W deployable radiator with loop heat pipe (SAE International, 2001). <https://doi.org/10.4271/2001-01-2194>.
13. Lashley, C., Krein, S. & Barcomb, P. Deployable radiators-A multi-discipline approach. Report No. 0148-7191, (SAE Technical Paper, 1998).
14. Zhao, H., Sun, Q., Zhou, J., Deng, X. & Cui, J. Switchable cavitation in silicone coatings for energy-saving cooling and heating. *Advanced Materials* **32**, 2000870, (2020). <https://doi.org/10.1002/adma.202000870>.
15. Xia, Z., Fang, Z., Zhang, Z., Shi, K. & Meng, Z. Easy way to achieve self-adaptive cooling of passive radiative materials. *ACS Applied Materials & Interfaces* **12**, 27241-27248, (2020). <https://doi.org/10.1021/acsami.0c05803>.
16. Nagano, H., Nagasaka, Y. & Ohnishi, A. Simple deployable radiator with autonomous thermal control function. *Journal of thermophysics and heat transfer* **20**, 856-864, (2006). <https://doi.org/10.2514/1.17988>.
17. Ono, M., Chen, K., Li, W. & Fan, S. Self-adaptive radiative cooling based on phase change materials. *Opt. Express* **26**, A777-A787, (2018). <https://doi.org/10.1364/OE.26.00A777>.
18. Chen, M., Morsy, A. M. & Povinelli, M. L. Design of VO_2-coated silicon microspheres for thermally-regulating paint. *Opt. Express* **27**, 21787-21793, (2019). <https://doi.org/10.1364/OE.27.021787>.

19. Taylor, S., Yang, Y. & Wang, L. Vanadium dioxide based Fabry-Perot emitter for dynamic radiative cooling applications. *Journal of Quantitative Spectroscopy and Radiative Transfer* **197**, 76-83, (2017). <https://doi.org/10.1016/j.jqsrt.2017.01.014>.
20. Zhang, W.-W., Qi, H., Sun, A.-T., Ren, Y.-T. & Shi, J.-W. Periodic trapezoidal VO_2-Ge multilayer absorber for dynamic radiative cooling. *Opt. Express* **28**, 20609-20623, (2020). <https://doi.org/10.1364/OE.396171>.
21. Ito, K., Watari, T., Nishikawa, K., Yoshimoto, H. & Iizuka, H. Inverting the thermal radiative contrast of vanadium dioxide by metasurfaces based on localized gap-plasmons. *APL Photonics* **3**, 086101, (2018). <https://doi.org/10.1063/1.5025947>.
22. Nishikawa, K., Yatsugi, K., Kishida, Y. & Ito, K. Temperature-selective emitter. *Applied Physics Letters* **114**, 211104, (2019). <https://doi.org/10.1063/1.5091048>.
23. Kim, H., Cheung, K., Auyeung, R. C. Y., Wilson, D. E., Charipar, K. M., Piqué, A. & Charipar, N. A. VO_2-based switchable radiator for spacecraft thermal control. *Scientific Reports* **9**, 11329, (2019). <https://doi.org/10.1038/s41598-019-47572-z>.
24. Sun, K., Riedel, C. A., Urbani, A., Simeoni, M., Mengali, S., Zalkovskij, M., Bilenberg, B., de Groot, C. H. & Muskens, O. L. VO_2 thermochromic metamaterial-based smart optical solar reflector. *ACS Photonics* **5**, 2280-2286, (2018). <https://doi.org/10.1021/acsphotonics.8b00119>.
25. Morin, F. J. Oxides which show a metal-to-insulator transition at the neel temperature. *Physical Review Letters* **3**, 34-36, (1959). <https://doi.org/10.1103/PhysRevLett.3.34>.
26. Lee, S., Hippalgaonkar, K., Yang, F., Hong, J., Ko, C., Suh, J., Liu, K., Wang, K., Urban, J. J., Zhang, X., Dames, C., Hartnoll, S. A., Delaire, O. & Wu, J. Anomalously low electronic thermal conductivity in metallic vanadium dioxide. *Science* **355**, 371-374, (2017). <https://doi.org/10.1126/science.aag0410>.
27. Barker, A. S., Verleur, H. W. & Guggenheim, H. J. Infrared optical properties of vanadium dioxide above and below the transition temperature. *Physical Review Letters* **17**, 1286-1289, (1966). <https://doi.org/10.1103/PhysRevLett.17.1286>.
28. Agassi, J. The Kirchhoff-Planck radiation law. *Science* **156**, 30-37, (1967). <www.jstor.org/stable/1720913>.
29. Rosado, P. J. & Levinson, R. Potential benefits of cool walls on residential and commercial buildings across California and the United States: Conserving energy, saving money, and reducing emission of greenhouse gases and air pollutants. *Energy and Buildings* **199**, 588-607, (2019). <https://doi.org/10.1016/j.enbuild.2019.02.028>.
30. EIA, Structural and Geographic Characteristics of U.S. Homes by Housing Unit Type, 2015. https://www.eia.gov/consumption/residential/data/2015/hc/php/hc2.1.php

Materials and Methods

Preparation of the TARC

675 µm-thick Si wafers were first covered with ~ 2 µm thick polyimide film (PI-2545, HD MicroSystems LLC) via spin coating, which was then cured in a N_2-filled oven at 425 °C for 60 minutes. The polyimide film acts as an etching protection layer for the final transfer process. $W_xV_{1-x}O_2$ thin films were grown on the polyimide layer using pulse laser deposition (PLD). The PLD target was prepared by mixing WO_3 and V_2O_5 powders with W:V atomic ratio at 1.5%, then made into 2.5 cm diameter round discs with a hydraulic press. All $W_xV_{1-x}O_2$ thin films were deposited in 5 mTorr O_2 environment at 500 °C substrate temperature, and the PLD laser energy was set at 321 mJ with 10 Hz pulse frequency. 70 nm of $W_xV_{1-x}O_2$ was grown at a rate of 6 nm/min, followed by a post-

deposition anneal at 500 °C for 30 mins in the same 5 mTorr O_2 environment. The metamaterials patterns were made with standard photolithography, combined with etching of $W_xV_{1-x}O_2$ by $SF_6 + O_2$ in a plasma etching system. After removing the photoresist with acetone and O_2 plasma, 1.5 μm thick BaF_2 and 100 nm thick Ag layers were grown sequentially on top via thermal evaporation. The growth rates of BaF_2 and Ag were controlled at 20 Å/s and 2 Å/s, respectively.

In the transfer process, a piece of 0.06 mm thick single-sided sticky cellophane packaging tape was first carefully applied to fully cover the surface, where the Ag layer was stuck to the adhesive side without any residual air bubbles. An initial Si substrate removal process was performed in a $HF + HNO_3$ solution, mixed by aqueous HF (49% weight percentage) and HNO_3 solution (68% weight percentage) with a volume ratio of 10:1. The samples were pulled out and rinsed with DI water to stop the initial etching when the etchant starts to touch down on the polyimide layer. A XeF_2 dry etching process was then carried out to clean off the residue Si. In the final step, the polyimide protection layer was removed by O_2 plasma at 100 mTorr O_2 pressure and 200 W plasma power for ~ 11 mins.

Spectrally resolved measurements

Thermal spectral reflectance at normal incidence $r(\lambda, T)$ was characterized by a Nicolet iS50 FTIR spectrometer and Nicolet Continuum microscope over the spectrum 5 – 15 μm. The objective lens was 32× with 0.65 numerical aperture. A blade aperture of 100 μm × 100 μm was used to select the area of interest. All reflection spectra were normalized to the reflection spectrum of a 300 nm thick gold film. The temperature of the samples (ranging from 15 °C to 50 °C) was controlled by a customized closed-loop thermal stage, connected to a Lakeshore 321 temperature controller. Applying Kirchoff's law of radiation, thermal spectral emittance $\varepsilon(\lambda, T)$ was computed as $\varepsilon(\lambda, T) = a(\lambda, T) = 1 - r(\lambda, T)$ since the TARC was essentially opaque from 5 to 15 μm.

Near normal-hemispherical solar spectral reflectance $r(\lambda)$ was measured from 300 to 2,500 nm with an Agilent Cary 5000 UV-vis-NIR spectrometer equipped with an Internal Diffuse Reflectance Accessory (DRA-2500), which collects both specular and diffuse reflections. Solar spectral absorptance was computed as $a(\lambda) = 1 - r(\lambda)$since the film was essentially opaque to sunlight.

The solar absorptance *A* and sky-window thermal emittance ε_s can be calculated from the corresponding spectral data by:

$$A = \left(\int_{0.3}^{2.5\,\mu m} I_s(\lambda) a(\lambda) d\lambda \right) / \left(\int_{0.3}^{2.5\,\mu m} I_s(\lambda) d\lambda \right)$$

$$\varepsilon_s(T) = \left(\int_{8}^{13\,\mu m} B(\lambda) \varepsilon(\lambda, T) d\lambda \right) / \left(\int_{8}^{13\,\mu m} B(\lambda) d\lambda \right)$$

In which $I_s(\lambda)$ is the solar spectral intensity, and $B(\lambda)$ is the spectral radiance of black body.

Thermal infrared imaging and analysis

The TIR images were captured by a FLIR ONE infrared camera working at a wavelength range of 8-13 μm. To minimize the reflection signals from the camera and the surroundings, the default viewing angle was set as 15° instead of normal incident direction, and the experiments were performed in an open-area, outdoor environment under clear sky (cloud-free). When taking IR images, the camera measures the incident thermal radiation, and then gives the temperature reading (T_{TIR}) assuming a constant thermal emittance for the target (e.g., $\varepsilon_0 = 0.90$, default setting of the camera).

Simulation of device properties

The spectral absorptance of TARC is numerically calculated using COMSOL Multiphysics, with all the geometric parameters matching the original design. Material properties in IR and visible ranges are from [1-3] and [4-6], respectively.

Simulation of surface temperature

The stabilized temperature of a surface (T_s) with given solar absorptance (A) and thermal emittance (ε) was calculated based on adiabatic approximation, assuming negligible heat transfer between the surface and the underlying structure. The key climate parameters for a specific city or region, including air temperature (T_a), dew point temperature (T_d), wind speed (v), solar radiance (I) and cloud coverage factor (CF) are obtained from the open source data base[7] using the TMY3 weather files. The thermal emittance of the TARC was set at 0.20 for T_s < 19 °C and 0.90 for T_s > 27 °C, and approximated by a linear interpolation in the transition region (27 °C > T_s > 19 °C). Based on this setup, the all-year-around temperature map (Fig. 4C) of TARC and of conventional materials with an arbitrary combination of static A and ε were calculated and compared. More details of the simulation can be found in the Supporting information.

Projection of energy savings

Rosado & Levinson[8] simulated the annual space heating source energy savings ΔS_h (typically negative) and the annual space cooling source energy savings ΔS_c (typically positive) attained by increasing roof albedo for various categories and vintages of buildings in 15 U.S. climates zones and 16 California climate zones. Note that $\Delta S_h$and ΔS_c are not directly presented in Rosado & Levinson but can be estimated from the heating, cooling, and fan energy uses reported in that work, as described in SI Appendix I.

Summing ΔS_h and ΔS_c yields the annual space-conditioning (heating + cooling) source energy savings ΔS. We used U.S. cool-roof energy savings reported by Rosado & Levinson and our own calculations of to the hourly roof surface temperature to regress ΔS_h to reduction ΔD_hin annual average heating degrees D_h, and ΔS_c to reduction ΔD_c in annual average cooling degreesD_c. These linear fits of the form $\Delta S_h = \alpha_h \Delta D_h$ and $\Delta S_c = \alpha_c \Delta D_c$ yield $\Delta S = ¿\, \alpha_h \Delta D_h + \alpha_c \Delta D_c$. Specifically, energy simulations for four static roofing materials with E=0.90 and solar reflectance R=0.10, 0.25, 0.40, or 0.60 (

$A = 1 - R = 0.90$, 0.75, 0.60, or 0.40¿ were selected for the extraction of the coefficients α_h and α_c using the material with A = 0.90 as the baseline.

To evaluate the potential space-conditioning source energy savings (SCSES) obtained by using TARC instead of a reference roofing surface of static solar absorptance A_{ref} and static thermal emittance ε_{ref}, we calculated in each city $\Delta D_{h,TARC}(A_{ref}, \varepsilon_{ref}) \equiv D_{h,TARC} - D_h(A_{ref}, \varepsilon_{ref})$ and $\Delta D_{c,TARC}(A_{ref}, \varepsilon_{ref}) \equiv D_{c,TARC} - D_c(A_{ref}, \varepsilon_{ref})$ varying A_{ref} and ε_{ref} from 0 to 1.00. We then computed space-conditioning source energy savings $\Delta S_{TARC}(A_{ref}, \varepsilon_{ref})$¿ $\alpha_h \Delta D_{h,TARC}(A_{ref}, \varepsilon_{ref}) + \alpha_c \Delta D_{c,TARC}(A_{ref}, \varepsilon_{ref})$ over this space for each building category and vintage of interest. The minimum $\Delta S_{TARC}(A_{ref}, \varepsilon_{ref})$ (namely, $SCSES_{min}$) for all possible existing roof coating properties is taken as the figure of merit for each combination of local climate, building category and vintage group.

Acknowledgements. This work was supported by the Electronic Materials Program in the Lawrence Berkeley National Laboratory, which is supported by the Director, Office of Science, Office of Basic Energy Sciences, Materials Sciences and Engineering Division, of the U.S. Department of Energy under Contract No. DE-AC02-05CH11231. J.W. acknowledges support from the Bakar Prize. R.L. acknowledges support of the Assistant Secretary for Energy Efficiency and Renewable Energy Building Technologies Office of the U.S. Department of Energy under Contract No. DE-AC02-05CH11231.

References

1. Ordal, M. A., Bell, R. J., Alexander, R. W., Long, L. L. & Querry, M. R. Optical properties of fourteen metals in the infrared and far infrared: Al, Co, Cu, Au, Fe, Pb, Mo, Ni, Pd, Pt, Ag, Ti, V, and W. Appl. Opt. 24, 4493-4499, (1985). <https://doi.org/10.1364/AO.24.004493>.
2. Dong, K., Hong, S., Deng, Y., Ma, H., Li, J., Wang, X., Yeo, J., Wang, L., Lou, S., Tom, K. B., Liu, K., You, Z., Wei, Y., Grigoropoulos, C. P., Yao, J. & Wu, J. A lithography-free and field-programmable photonic metacanvas. Advanced Materials 30, 1703878, (2018). <https://doi.org/10.1002/adma.201703878>.
3. Qazilbash, M. M., Brehm, M., Andreev, G. O., Frenzel, A., Ho, P. C., Chae, B.-G., Kim, B.-J., Yun, S. J., Kim, H.-T., Balatsky, A. V., Shpyrko, O. G., Maple, M. B., Keilmann, F. & Basov, D. N. Infrared spectroscopy and nano-imaging of the insulator-to-metal transition in vanadium dioxide. Physical Review B 79, 075107, (2009). <https://doi.org/10.1103/PhysRevB.79.075107>.
4. Johnson, P. B. & Christy, R. W. Optical constants of the noble metals. Physical Review B 6, 4370-4379, (1972). <https://doi.org/10.1103/PhysRevB.6.4370>.
5. Kana Kana, J. B., Vignaud, G., Gibaud, A. & Maaza, M. Thermally driven sign switch of static dielectric constant of VO2 thin film. Optical Materials 54, 165-169, (2016). <https://doi.org/10.1016/j.optmat.2016.02.032>.
6. Malitson, I. H. Refractive properties of barium fluoride. JOSA 54, 628-632, (1964). <https://doi.org/10.1364/JOSA.54.000628>.
7. EnergyPlus, Weather Data by Region. Downloaded from https://energyplus.net/.
8. Rosado, P. J. & Levinson, R. Potential benefits of cool walls on residential and commercial buildings across California and the United States: Conserving energy, saving

526 money, and reducing emission of greenhouse gases and air pollutants. Energy and
527 Buildings 199, 588-607, (2019). <https://doi.org/10.1016/j.enbuild.2019.02.028>.